Synchronous phase demodulation algorithm for conic carrier Hartmann topographer

A. Gonzalez[a,*], M. Rivera[b], M. Servin[a], Ricardo Legarda-Saenz[c], Oscar Dalmau[b], Amalia Martínez[a]

[a] *Centro de Investigaciones en Óptica A. C., Loma del Bosque 115, 37150 León Guanajuato, México*
[b] *Centro de Investigacioń en Matemáticas A. C., Jalisco S/N Col. Valenciana, 36240 Guanajuato Guanajuato México*
[c] *Facultad de Matemáticas, Universidad Autónoma de Yucatán, Cordemex 172, 97110, Mérida Yucatán México*

Abstract

In this paper, a theoretical analysis of a new algorithm for measuring phase objects (PO) is presented. The algorithm analyses images captured with a modified Hartmann plate. The proposed method demodulates a signal with a conic-wavefront carrier by using synchronous interferometric techniques. Typically a Hartmann Plate is a mask with an array of holes, the proposal is to replace those holes with a series of circular concentric rings created by a conic carrier, named Conic Hartmann Plate mask (CHM). The proposed algorithm computes a dense correspondence between the pattern source and its interferogram on the PO. This dense correspondence is computed as the phase change of the refracted waveform with respect to the reference one. This approach is more robust than standard techniques that computes the centroid of each spot in order to estimate its position; which involves pattern recognition and segmentation tasks, something normal in a typical Hartmann test. We show in this work that the new method overcomes different problems such as irregular background illumination, spots overlapping with pupil border and spots matching due to rapid changes on the surface slopes. This work shows a general procedure for radial derivatives integration based on base functions. As far as the authors know, the here presented demonstration has not been reported before. In particular, we show that Zernike polynomials are suitable for PO. Numerical experiments with real and simulated data demonstrate the algorithm performance.

Keywords:
Fringe analysis

*Corresponding author
Email addresses: adonai.gonzalez@cio.mx (A. Gonzalez), mrivera@cimat.mx (M. Rivera), mservin@cio.mx (M. Servin), rlegarda@uady.mx (Ricardo Legarda-Saenz), dalmau@cimat.mx (Oscar Dalmau), amalia@cio.mx (Amalia Martínez)

1. Introduction

The use of methods that apply a mask with a series of circular equally–spaced concentric rings is not new in optical interferometry [1, 2, 3, 4, 5]. The combination of those kind of circular masks with others techniques such as Moiré or shearing techniques have been developed through years [6, 7, 8, 9, 10]. Those methods demand of computer-aided fringe pattern analysis, and in many cases the complexity of the fringe pattern requires of sophisticated algorithms [11, 12, 13, 14]. In addition, complex experimental setups are generally required. In this work, the experiments and numerical simulations are focused on the analysis of optics lenses. By using a Conic Hartmann Mask (CHM) and the proposed algorithm, it is possible to obtain the output wavefront of a lens. In fact, the work principle is based on the deflectometric technique, where a CHM is deformed by the phase object and the fringe pattern is imaged by a camera, this idea in combination with circular mask has been reported in the past [15, 16, 17]; Figure 1 depicts the experimental setup. In this technique, the captured image is phase-modulated by the lens irregularities. Hence, geometrical aberrations of the lens can be identified. The phase-modulated pattern allows the estimation of the radial slope of the lens with respect to its closest sphere. In the traditional Hartmann test, the accuracy of the curvature estimation is a function of the number of spots identified over the object. To increase the number of estimated slope-points some authors have proposed more complicated radial symmetric pattern masks [18, 19, 20]. In contrast, synchronous interferometric methods used in optical metrology provide a dense phase estimation (*i.e.*, at every pixel of the fringe pattern domain) [21]. Interferogram analysis implies a demodulation process of the recorded information, where each interferogram needs its own specific reference carrier for an appropriate demodulation; for example, linear demodulation uses a plane-wavefront (carrier) as reference [22]. This paper presents a new digital interferometric method for interferogram demodulation which uses conic-carrier. Additionally, we propose, a general, basis–function based procedure for recovering smooth wavefronts (exempt for a constant term) from radial derivative. As far as the authors known, the here presented demonstration has not been reported before. As example, we show that Zernike Polynomials can properly be used for this integration task. The performance of the method is demonstrated by numerical experimental results.

2. Synchronous demodulation of modulated interferograms with equal-spaced concentric rings

In this work we assume that our Conic Hartmann Mask (CHM) has a continuous cosine (radial) transmittance profile. Thus, let P be the observed fringe

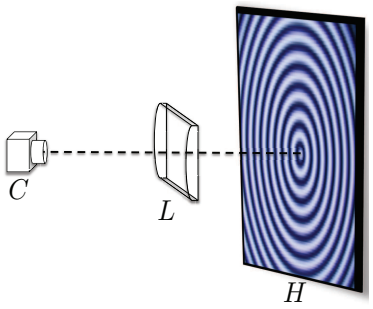

Figure 1: Schema of the experimental setup for Conic Hartmann Mask (CHM): conic carrier Hartmann mask (H), test lens (L) and camera (C).

(CHM) pattern and let $x = [x_1, x_2]^T$ be the image pixel coordinates with number of rows M and number of columns N. Hence, by assuming the fringe–pattern origin is the image central–pixel $x^0 = [x_1^0, x_2^0]^T$, the transformation of x to polar coordinates (ρ, θ) is given by the Euclidean distance (radio),

$$\rho = \frac{\|x - x^0\|_2}{\frac{1}{2}\min\{M, N\}}\,, \tag{1}$$

and the angular position, $\theta = \angle(x - x^0)$. Therefore, the model of CHM in polar coordinates is

$$CHM(\rho, \theta) = 1 + \cos\left(\omega_0 \rho\right)\,, \tag{2}$$

where $\omega_0 = 2\pi\kappa$ is the spatial frequency and κ is the number of fringes into the interval $\rho \in [0, 1]$. The CHM in Eq. (2) is phase-modulated by a test–subject with slope changes corresponding to the physical variable of interest; such as wavefront aberrations. The resulted phase-modulated CHM image is modelled by:

$$I(\rho, \theta) = a(\rho, \theta) + b(\rho, \theta)\cos\left(\omega_0 \rho + s\,\phi_\rho\right); \tag{3}$$

where, $a(\cdot, \cdot)$ is the background illumination, $b(\cdot, \cdot)$ is the contrast, s is a scale value that depends on the experimental geometry and

$$\phi_\rho(\rho, \theta) \stackrel{def}{=} \frac{\partial \phi(\rho, \theta)}{\partial \rho}\,, \tag{4}$$

is the partial derivative of the output wavefront ϕ, with respect to (*w.r.t.*) the radial position ρ, [23, 24, 25, 26]. In the literature, ϕ_ρ is named the *radial-slope*. Next, we present our proposal of a synchronous detection algorithm with conic carrier to computing an estimation of ϕ_ρ and, after, we present the radial integration procedure. A preliminary version of this demodulation step was reported in [27].

First, we multiply Eq. (3) by the complex conic-wavefront reference, $\exp\left(-\imath\omega_0\rho\right)$. This reference pattern has the same spatial frequency and its circular fringes

center matches the center of the CHM image I. Therefore, by decomposing the cosine signal in two complex exponentials, we obtain:

$$
\begin{aligned}
I(\rho,\theta)\exp\left(-\imath\omega_0\rho\right) &= a(\rho,\theta)\exp\left(-\imath\omega_0\rho\right) && (5)\\
&\quad +\frac{1}{2}b(\rho,\theta)\exp\left[-\imath(2\omega_0\rho+s\,\phi_\rho(\rho,\theta))\right] && (6)\\
&\quad +\frac{1}{2}b(\rho,\theta)\exp\left[-\imath s\,\phi_\rho(\rho,\theta)\right]. && (7)
\end{aligned}
$$

We can observe that the three terms in the right side of Eqs. (5) to (7) can be understood as follows. The analytic signal of the conic-wavefront (Eq. (5)), corresponds to a ring in Fourier space with radius ω_0 convolved with the spectrum of the low frequency pattern background, a; see Figure 2. The analytic signal of the conic-wavefront with twice the reference carrier (Eq. (6)) corresponds in the Fourier space to a ring with radius $2\omega_0$ convolved with the spectrum of the low frequency pattern contrast, b; see Figure 2. The complex exponent of the desired analytical signal is represented in the Fourier space by a central spot, which phase component contains the desired information ϕ_ρ; see Figure 2.

We note from Figure 2 that ϕ_ρ can be estimated by means of a low pass filtering process which preserves the central lobule. We denote by L a low-pass filter that rejects the two high frequency terms associated with the conic wavefronts Eqs. (5) and (6); *i.e.*,

$$
\begin{aligned}
\tilde{I}(\rho,\theta) &= L\left[I(\rho,\theta)\exp\left(-\imath\omega_0\rho\right)\right]\\
&= \frac{1}{2}b(\rho,\theta)\exp\left[-\imath s\,\phi_\rho(\rho,\theta)\right]\,, && (8)
\end{aligned}
$$

where $\tilde{I}$ denotes the filtered CHM modulated pattern. The proposed demodulation algorithm, for CHM images, is based on Eq. (8). The algorithm is only restricted by the capability of having a well defined separation base-band in the analytical signal expressed by Eqs. (5) to (7) [28]. Then, an estimation of the radial slope-value $\hat{\phi}_\rho$ for each pixel can be calculated as:

$$
\hat{\phi}_\rho(\rho,\theta) = \frac{1}{s}\arg[\tilde{I}(\rho,\theta)], \tag{9}
$$

where the function $\arg(x+\imath y):\mathbb{C}\to[-\pi,\pi)$ computes the phase of a complex number: the computed phase is wrapped.

Different from standard Hartmann test analysis, which is based on image intensity, the proposed algorithm computes a dense (at each pixel) estimation of the radial–slope from Eq. (9).

3. Base functions for spatial integration of radial slope fields

Any continuous smooth two–dimensional (2D) function can be expressed as lineal combination of smooth based functions; for example, we can use Zernike

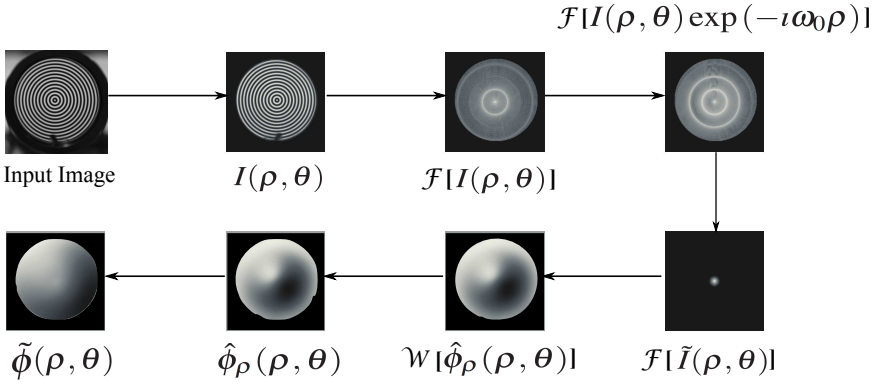

Figure 2: Block diagram of the proposed demodulation algorithm for CHM images by using digital interferometry. A real lens is used as the object under test which is modulated by using a CHM. As it is explained in this section, the frequency spectrum decomposition (using *Fourier Transform* $\mathcal{F}[.]$) allows the application of a low pass-filter in order to obtain an estimation of the wrapped phase ($\mathcal{W}[.]$). After this, an unwrapping process is computed followed by the integration scheme based on the use of Zernike polynomials.

polynomials for functions defined within the unit circle [29]. In particular, the smooth radial derivative, ϕ_ρ, can be expressed as the sum of smooth basis functions, in polar coordinates, as:

$$\phi_\rho(\rho,\theta) = \sum_{j=1}^{n} a_j \Psi_j(\rho,\theta)\,; \tag{10}$$

for $\rho \in [0,1], \theta \in [0,2\pi)$ and n *sufficiently large*. By abusing of the notation, this formula can be written in matrix form as $\phi_\rho = \mathbf{\Psi} a$, where ϕ_ρ denotes, now, a column vector of length equal MN, $\mathbf{\Psi} = [\Psi_j]_{j=1,2,\ldots,n}$ and the column vector $\Psi_j \in \mathbb{R}^{MN}$ denotes the discretisation of the jth basis function.

One advantage of the dense and regular radial derivative ϕ_ρ is that the number MN of samples (pixels) in the unitary circle is large and equally–spaced. Since one can not guarantee orthogonality on a discretisation of continuos orthogonal base functions, we estimate the a coefficients with a least squares procedure:

$$\tilde{a} = \text{argmin}_a \, \|\mathbf{\Psi} a - \phi_\rho\|_2^2 \,. \tag{11}$$

Once we compute a, we can be obtain ϕ by the definite integral of Eq. (10):

$$\phi(\rho,\theta) = \int_0^\rho \phi_\rho(r,\theta)\, dr = C(0,\theta) + \sum_{j=1}^{n} a_j \hat{\Psi}_j(\rho,\theta)\,; \tag{12}$$

where, by continuity, $C(0,\theta) = C$ independently of the angle θ. This constant C is a piston term that can be neglected because it does not affect the phase shape. Moreover, the columns of $\hat{\mathbf{\Psi}} = [\hat{\Psi}_j]_{j=1,2,\ldots,N}$ denote the analytical integrals of

the corresponding (Zernike) base functions:

$$\hat{\Psi}_j(\rho,\theta) = \int \Psi_j(\rho,\theta)\, d\rho. \tag{13}$$

We can write Eq. (12) in matrix form:

$$\tilde{\phi} = \hat{\mathbf{\Psi}}\tilde{a}; \tag{14}$$

where $\tilde{\phi}$ is the final estimation of the phase ϕ. Eqs. (11) and (14) resume the radial integration procedure.

4. Experiments of Phase Demodulation

The algorithm presented in this paper estimates the elevation deviation of the tested surface respect to a sphere. The technique's performance is demonstrated with a real lens and numerical simulations. Figure 3(a) shows the original CHM pattern, before passing through the lens. Figure 3(b) shows the image of the same CHM modulated by the lens, after passing through the lens. Figure 3(c) shows the magnitude of the*Fourier Spectra Transform* of Figure 3(b) after applying Eq. (8).

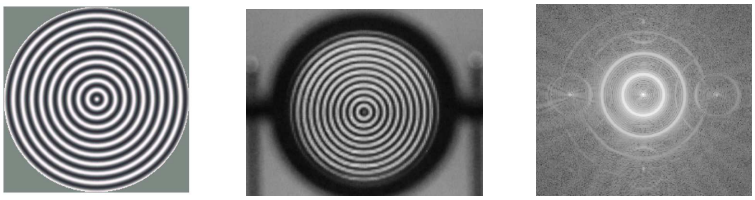

(a) (b) (c)

Figure 3: (a) Original CHM pattern made of on a set of equally spaced rings. (b) Phase-Modulated CHM pattern by the lens. Here a phase variations produced by the lens surface is observed as a deformation of the rings. (c) Fourier Spectrum of the Phase-Modulated CHM pattern.

By the use of the interferometric demodulation algorithm proposed in this paper, the two conjugate spectra are well base–band separated, as it can be seen in Figure 3(c). The brightly central spot represents the analytic signal: $b(\rho,\theta)\exp\left[-\imath s\,\phi_\rho(\rho,\theta)\right]$. The two other rings surrounded this central spot correspond to the terms expressed by Eqs. (5) and (6), as it is presented in Eqs. (5) to (7). We compare the performance of our method with the newest one reported in [11]. Figures 4(a) to 4(c) show the results of applying the Variational method and the proposed one.

As it can be noted, the computed result with the Variational method still has contributions of the conic-carrier; *i.e.*, some low-contrast rings are presented in the reconstructed wavefront. The carrier used in the CHM algorithm is a synthetic estimation of the original.

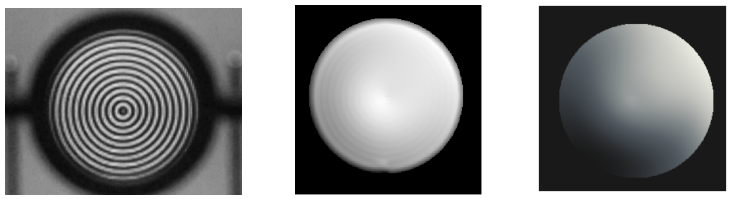

(a) (b) (c)

Figure 4: (a) CHM Phase-Modulated CHM pattern by the lens: the phase variations produced by the lens surface produce rings distortions. (b) Analysis of the output wavefront with the variational method. (c) Analysis of the output wavefront with the CHM method.

Error in the estimation of the fringes center and their spatial frequency may introduce an error in the estimated phase. For this reason, we compute the center coordinates as the mass center of the section that contains the first radial ring. We also determine the fringe number by simple inspection of the image. Two numerical experiments, using a reference sphere, were performed in order to estimate errors due to a miscalculation in the number of fringes and the center position of the synthetic carrier used for synchronous demodulation. The numerical simulation let to know the exact position of the center of the CHM, from this position, the synthetic conic carrier was translated six pixels in the x and y image coordinate system, after this the Mean Square Error (MSE) is computed. The results can be observed in Figure 5(a). The number of fringes can be set in the CHM as a known value for the numerical experiment, variations from less than 5 fringe to more than 5 fringe from the original value are introduced for the construction of the synthetic conic carrier, for each synthetic conic carrier with its own number of fringes, the MSE is computed. The results can be observed in Figure 5(b).

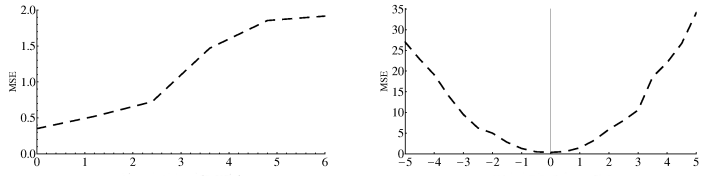

(a) Center position *vs.* MSE (b) Fringe number *vs.* MSE

Figure 5: Error in the estimated phase produced by wrong estimations of the center position or the fringe number.

In order to validate the proposed method, seven numerical experiments were carried out. For all the experiments presented here, the number Zernike polynomials used was fixed to 100. The result of the integration process gives the output wavefront. The first four experiments are based on the functions previously reported by Trevino *et. al.* [30]. The last three test wavefronts are

generated by Zernike polynomial compositions. The explicit functions are:

$$\phi_1(\rho,\theta) = \exp\left[-\frac{0.09-0.6\rho\cos(\theta)+0.01-0.2\rho\sin(\theta)+\rho^2}{0.18}\right], \quad (15)$$

$$\phi_2(\rho,\theta) = \exp\left[-\frac{(\rho-0.54)^2}{0.04}\right], \quad (16)$$

$$\phi_3(\rho,\theta) = \exp\left[-\left(\frac{\theta-0.55}{3}\right)^{10}\right]\phi_2(\rho,\theta), \quad (17)$$

$$\phi_4(\rho,\theta) = \rho^5\exp\left[-\left(\frac{5\rho}{4}\right)^2\right], \quad (18)$$

$$\phi_5(\rho,\theta) = r^2\cos(\theta), \quad (19)$$

$$\phi_6(\rho,\theta) = \sqrt{2}\left(2r^2 + r\left(2r^2\left(2\left(5r^2-6\right)\sin(\theta)+\cos(3\theta)\right)+\sqrt{5}\left(15r^4-20r^2+6\right)r\cos(2\theta)+6\sin(\theta)\right)-1\right)+2r\cos(\theta), \quad (20)$$

$$\phi_7(\rho,\theta) = r\left(\sqrt{6}\left(3r^2-2\right)\sin(\theta)+2\sqrt{2}\left(10r^4-12r^2+3\right)\cos(\theta)+2\sin(\theta)\right). \quad (21)$$

The functions Eqs. (15) to (21) were tested by using a simulation of the Hartmann test, the variational method proposed by Legarda *et. al* [11] and the proposed method. The results are shown in Figure 6. We use the MSE for comparing the quality of the method, see results in Table 1.

Computed MSE for the tested surface ($\times 10^{-2}$)							
METHOD	ϕ_1	ϕ_2	ϕ_3	ϕ_4	ϕ_5	ϕ_6	ϕ_7
H	13.25	17.67	19.28	14.57	7.58	11.55	13.47
V	7.18	**0.53**	1.52	**0.03**	0.42	1.32	3.22
P	**0.43**	1.12	**0.88**	0.30	**0.36**	**0.22**	**1.05**

Table 1: MSE of the recovered phases with Hartmann (H), Variational (V) and proposed (P) methods using the test functions in Eqs. (15) to (21); best result remarked in bold.

Figure 6 presents the results of the three different phase recovering method using the test functions in Eqs. (15) to (21). The Variational (V) method and the proposed (P) here, offer the best approach to the original function. In contrast, the Hartmann (H) test is more robust than the Variational when notorious changes in θ are present. This is why the MSE is lower in the CHM technique. On other hand, when the test object is a flat surface, or more specific, when the angular-derivative component of the object under test is small, the Variational method has the lower MSE. This behavior is due the assumption of the Variational method that assumes that changes in θ tend to zero. Although variants of our approach has been discussed by previous works [32, 33, 34], in the best of our knowledge, this is the first time that a proof of the correctness of the integration procedure is presented.

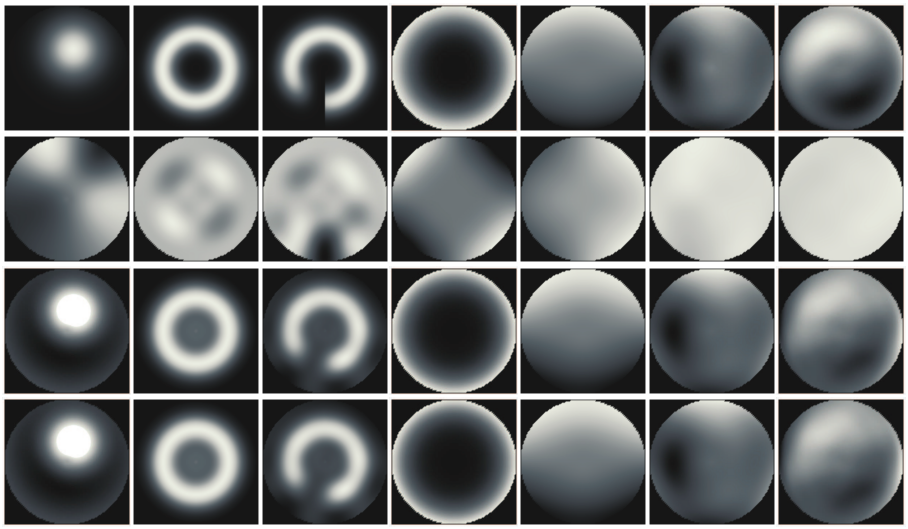

Figure 6: First row: test functions defined in Eqs. (15) to (21). Reconstructions computed with Hartmann test (second row), Variational method (third row) and proposed method (last row).

5. Conclusions

We present a new synchronous digital interferometric method for phase-demodulation of concentric-rings images. Our method is based on the use of a conic–carrier reference to demodulate CHM image pattern. The result of this phase demodulation corresponds to the wavefront estimation of the phase object under study. A major advantage of our method is that we use the information provides by all the pixels in the image, in contrast to the Hartmann test in which the results are supported by a sparse point-set. We show that an estimation of the CHM modulated waveform in the *Fourier space*, can be obtained through the densely computed radial slope, ϕ_ρ. A special focus of the sensibility on radial-slope detection depends on the accuracy of the conic-carrier center position. An inadequate selection of its central position derive in fake estimation of the corneal radial-slope. In other hand, the number of fringes in the conic carrier affects the assessment of the slope by adding a cone. Given that any lens surface is expected to be smooth, the lens wavefront is computed by fitting a set of base function to the radial derivative.As example, in our experiments, we use discretized Zernike polynomials. Then, te computed mixture coefficients can be used to compute the radial integration.

It is important to remark that, the main contribution of this paper is to present a new approach for analysing images based on the use of a CHM and the redial integration procedure. We note that the calibration procedure is out the scope this work, and it is intended as a future work.

6. Acknowledgments

We thank the support of the Consejo Nacional de Tecnologia (CONACYT).

References

[1] K. Patorski, K. Pokorski, and M. Trusiak, "Circular-linear grating Talbot interferometry with Moiré Fresnel imaging for beam collimation," Opt. Lett. 39(2), 291-294 (2014).

[2] Z. Bin, "Digital Moiré Fringe-Scanning Method for Centering a Circular Fringe Image," Appl. Opt. 43(14), 2833-2839 (2004).

[3] Hongyan Zhang, Cheng Wang, Xuemei Liu and Chunguang Liu, "Phase-shifting method for circular grating moire technique," Proc. SPIE 4231, Advanced Optical Manufacturing and Testing Technology 2000, 603 (October 6, 2000).

[4] M. Thakur, A. Vyas, and C. Shakher, "Measurement of Temperature Profile of a Gaseous Flame with a Lau Phase Interferometer that has Circular Gratings," Appl. Opt. 41(4), 654-657 (2002).

[5] C. Shakher and A. Daniel, "Talbot interferometer with circular gratings for the measurement of temperature in axisymmetric gaseous flames," Appl. Opt. 33(25), 6068-6072 (1994).

[6] D. Silva, "Talbot Interferometer for Radial and Lateral Derivatives," Appl. Opt. 11(11), 2613-2624 (1972).

[7] Y. Nakano and K. Murata, "Measurements of phase objects using the Talbot effect and moiré techniques," Appl. Opt. 23(14), 2296-2299 (1984).

[8] C. Shakher, S. Prakash, D. Nand, and R. Kumar,"Collimation Testing with Circular Gratings," Appl. Opt. 40(8), 1175-1179 (2001).

[9] N. Gu, L. Huang, Z. Yang, and C. Rao, "A single-shot common-path phase-stepping radial shearing interferometer for wavefront measurements," Opt. Express 19(5), 4703-4713 (2011).

[10] J. Wang, Y. Song, Z. Li, and A. He, "Two-step spatial phase-shifting radial shearing interferometery with circular gratings," Opt. Lett. 38(7), 1116-1118 (2013).

[11] Ricardo Legarda-Saenz, Carlos Brito-Loeza, Mariano Rivera, Arturo Espinosa-Romero, "Variational method for integrating radial gradient field", Optics and Lasers in Engineering, 63, 53-57 (2014).

[12] Bo Li, Lei Chen, Jiang Bian and Yan Li, "A demodulation method for the circular carrier interferogram using phase stitching," Optics and Lasers in Engineering, 49(9), 1118-1123 (2011).

[13] X. Meng, X. Peng, L. Cai, A. Li, J. Guo, and Y. Wang,"Wavefront reconstruction and three-dimensional shape measurement by two-step dc-term-suppressed phase-shifted intensities," Opt. Lett. 34(8), 1210-1212 (2009).

[14] M. Trusiak, K. Patorski, and K. Pokorski, "Hilbert-Huang processing for single-exposure two-dimensional grating interferometry," Opt. Express 21(23), 28359-28379 (2013).

[15] J. Massig, "Measurement of phase objects by simple means" Appl. Opt. 38, 4103-4105 (1999).

[16] Y. Mejía and D. Malacara, "A review of methods for measuring corneal topography," Optometry and vision science, 78(4), 240-253 (2001).

[17] O. A. Skydan, M. J. Lalor and D. R. Burton, "3D shape measurement of automotive glass by using a fringe reflection technique," Meas. Sci. Technol. 18, 106-114 (2007).

[18] E. J. Sarver, US Patent No. 7,938,537 (22 June 2010).

[19] T.N. Turner, G. D. Niven, J. R. Bentley, E. J. Sarver and C. R. Broadus, US Patent No. 5,864,383 (24 April 1997).

[20] D. Malacara-Doblado and I. Ghozeil, "Hartmann, Hartmann-Shack, and Other Screen Tests," in Optical Shop Testing, 3rd ed., D. Malacara ed., John Wiley & Sons, Inc. (2007).

[21] D. Malacara-Doblado, K. Creath, J. Schmit, and J. C. Wyant, "Testing of aspheric wavefronts and surfaces," in Optical Shop Testing 3rd ed., D. Malacara, ed., (Wiley, 2007) 435-497.

[22] M. Takeda, H. Ina, and S. Kobayashi, "Fourier-transform method of fringe-pattern analysis for computer based topography and interferometry," J. Opt. Soc. Am, 72, 156-160 (1982).

[23] Yukinobu Ban, US Patent No. 6,382,796 B1 (5 June 2000).

[24] D. C. Grove, US Patent No. 7,219,996 B2 (22 May 2007).

[25] L. A. Carvalho and J. C. Castro, "The Placido wavefront sensor and preliminary measurement on a mechanical eye," Optometry and Vision Science, 83, 108-118 (2006).

[26] L.A. Carvalho, "Absolute accuracy of Placido-based videokeratographs to measure the optical aberrations of the cornea," Optom Vis Sci. 81(8), 616-628 (2004).

[27] M. Servin, "Synchronous phase-demodulation of concentric-rings Placido mires in corneal topography and wavefront aberrometry (theoretical considerations)," ArXiv e-prints, 1204.1950 (2012).

[28] D. Malacara, M. Servin, and Z. Malacara, Interferogram analysis for Optical Testing, 2nd ed., CRC Press, Taylor and Francis Group, (2005).

[29] D. Malacara (Ed.). Optical shop testing, 2nd edn, Wiley, New York, 1992,

[30] Trevino Juan P., Gómez-Correa Jesus E., Iskander D. Robert and Chávez-Cerda Sabino, "Zernike vs. Bessel circular functions in visual optics," phthalmic and Physiological Optics, 33(4), 1475-1313 (2013).

[31] Alonso-Caneiro, David Iskander, D. Robert and Michael J. Collins, "Estimating corneal surface topography in videokeratoscopy in the presence of strong signal interference," IEEE Transactions on Biomedical Engineering 55(18), 2381-2387 (2008).

[32] C. McAlinden, M. McCartney, J. Moore, "Mathematics of Zernike polynomials: a review," Clin Experiment Ophthalmol. 39(8), 820-827 (2011).

[33] M.K. Smolek, S.D. Klyce, "Goodness-of-prediction of Zernike polynomial fitting to corneal surfaces," J. Cataract. Refract. Surg. 31(12), 2350-2355 (2005).

[34] L. Wang, D. Chernyak, D. Yeh, D.D. Koch, "Fitting behaviours of Fourier transform and Zernike polynomials," J. Cataract. Refract. Surg. 33(6), 999-1004 (2007).